Facile and Quantitative Activation of Dihydrogen by the Phosphinidene-Stabilized Cluster $Ru_4(CO)_{13}(\mu_3\text{-PPh})$: Synthesis and Spectroscopic and Structural Characterization of $(\mu\text{-H})_2Ru_4(CO)_{12}(\mu_3\text{-PPh})$

Françoise Van Gastel, John F. Corrigan, Simon Doherty, Nicholas J. Taylor, and Arthur J. Carty*

Guelph-Waterloo Centre for Graduate Work in Chemistry, Waterloo Campus, Department of Chemistry, University of Waterloo, Waterloo, Ontario, Canada N2L 3G1

Received April 21, 1992

The phosphinidene-stabilized butterfly cluster $Ru_4(CO)_{13}(\mu_3\text{-PPh})$ (**1**) has a square pyramidal nido Ru_4P skeleton with three ruthenium atoms and one phosphorus atom in a square face. The cluster **1** readily adds dihydrogen at room temperature and 1 atm pressure under photolytic conditions, affording $(\mu\text{-H})_2Ru_4(CO)_{12}(\mu_3\text{-PPh})$ (**2**) quantitatively. The dihydride **2** is stable in the solid state and in solution under H_2. It has been fully characterized by IR and ^1H, ^{31}P, and ^{13}C NMR spectroscopy and by an accurate single-crystal X-ray structural analysis. Crystal data for **2**: $C_{18}H_7O_{12}PRu_4$, triclinic, space group $P\bar{1}$, a = 10.059 (2) Å, b = 13.678 (3) Å, c = 18.093 (5) Å, α = 85.60 (2)°, β = 78.97 (2)°, γ = 88.65 (2)°; with Z = 4, there are two independent molecules in the asymmetric unit. The structure was solved and refined to R = 2.77% (R_w = 3.44%) on the basis of 9482 observed reflections ($F \geq 6.0\sigma(F)$). The molecular structure of **2** is closely related to that of **1**, with retention of the nido square pyramidal Ru_4P framework. The two hydride ligands, located along the Ru(1)–Ru(3) and Ru(3)–Ru(4) basal edges, result in a slight increase in the length of the bridged Ru–Ru bonds and a modest overall expansion of the cluster core but no major change in geometry. Under CO and cyclohexene, **2** can be converted back to **1**, with concomitant reduction of the olefin. In solution in hydrocarbon solvents and in the absence of H_2, **2** converts slowly but quantitatively to $(\mu\text{-H})_2Ru_3(CO)_9(\mu_3\text{-PPh})$ and $Ru_3(CO)_{12}$. Variable-temperature ^{13}C NMR spectra have revealed three different dynamic processes involving localized CO exchanges. The implications of these reactions for small-molecule activation by main-group stabilized transition metal clusters are discussed.

Introduction

The activation of dihydrogen by a polynuclear transition metal complex is a process of fundamental significance to synthetic and catalytic cluster chemistry. Many examples of reactions of dihydrogen with clusters have been described, and these processes have been reviewed.[1,2] Addition may occur at a single metal site presumably via mechanisms similar to dihydrogen activation in mononuclear systems[3] or at two metal centers via M–M bond cleavage[4] or addition to a metal–metal multiple bond.[5] For clusters with bound unsaturated hydrocarbon or hydrocarbyl groups, dihydrogen activation may lead to ligand transformations or displacement in processes related to steps in a catalytic hydrogenation sequence. For example, the trinuclear allenyl cluster $Ru_3(CO)_8(\mu_3\text{-}\eta^3\text{-}CH_2{=}C{=}CPr^i)(\mu\text{-}PPh_2)$ is converted rapidly into the $\mu_3\text{-}\eta^2$-alkyne complex $(\mu\text{-H})Ru_3(CO)_8(\mu_3\text{-}\eta^2\text{-}\|\text{-}CH_3C{\equiv}CPr^i)(\mu\text{-}PPh_2)$ in the presence of H_2.[6] Very few examples of reversible addition of dihydrogen have been described although recently reports of H_2 activation with skeletal rearrangement have appeared.[7] Mechanistically, very little information is available on cluster activation of dihydrogen. However Keister and co-workers have conclusively demonstrated that the reaction of the electron-precise triruthenium cluster $(\mu\text{-H})Ru_3(CO)_{10}(\mu\text{-MeCO})$ with H_2 involves dissociation of a CO ligand prior to rate-determining oxidative addition.[8]

Despite the variety of reaction modes accessible to polynuclear complexes, it is a surprising fact that very few clusters activate dihydrogen at ambient temperature and 1 atm of H_2.[7b,9-11] Furthermore, cluster fragmentation frequently occurs under the conditions necessary for hydrogenation. These facts impose severe limitations on the potential utility of clusters for catalytic hydrogenation processes.[12]

We are investigating in detail the extensive chemistry of the remarkable phosphinidene-stabilized cluster $Ru_4(CO)_{13}(\mu_3\text{-PPh})$ (**1**), a molecule with a square pyramidal nido Ru_4P framework which presents an open square Ru_3P face to incoming reagents.[13] The cluster **1** activates H_2 at 25 °C and 1 atm pressure under UV irradiation to yield $(\mu\text{-H})_2Ru_4(CO)_{12}(\mu_3\text{-PPh})$ (**2**) quantitatively. The thermal reaction proceeds in high yield without appreciable fragmentation at 60 °C in *n*-hexane. In this paper, we describe these reactions, the complete characterization of **2**, including a single-crystal X-ray study, and the conversion of **2** back to **1** under CO in the presence of cyclohexene.

Experimental Section

General Procedures. Solvents for reactions, chromatography, and crystallizations were distilled from appropriate drying agents before use. Photolysis experiments were carried out using a 450-W Hg lamp through a water-cooled quartz filter. This was immersed into a cylindrical (20

(1) Humphries, A. P.; Kaesz, H. D. *Prog. Inorg. Chem.* **1979**, *25*, 145.
(2) Davies, S. C.; Kablunde, K. J. *Chem. Rev.* **1982**, *82*, 153.
(3) Shapley, J. R.; Keister, J. B.; Churchill, M. R.; DeBoer, B. G. *J. Am. Chem. Soc.* **1975**, *97*, 4147.
(4) Geoffroy, G. L.; Epstein, R. A. *Inorg. Chem.* **1977**, *16*, 2795.
(5) (a) Chisholm, M. H. *ACS Symp. Ser.* **1981**, *155*, 17. (b) Curtis, M. D.; Messerle, L.; Fontinos, N. A.; Gerlach, R. F. *ACS Symp. Ser.* **1981**, *155*, 221.
(6) Nucciarone, D.; Taylor, N. J.; Carty, A. J. *Organometallics* **1988**, *7*, 127.
(7) (a) Mul, W. P.; Elsevier, C. J.; van Leijen, M.; Vrieze, K. *Organometallics* **1992**, *11*, 1877. (b) Hogarth, G.; Hadj-Bagheri, N.; Taylor, N. J.; Carty, A. J. *J. Chem. Soc., Chem. Commun.* **1990**, 1352.
(8) Bavaro, L. M.; Montangero, P.; Keister, J. B. *J. Am. Chem. Soc.* **1983**, *105*, 4977.
(9) Arif, A. M.; Bright, T. A.; Jones, R. A.; Nunn, C. M. *J. Am. Chem. Soc.* **1988**, *110*, 5389.
(10) Fjare, D. E.; Jensen, J. A.; Gladfelter, W. L. *Inorg. Chem.* **1983**, *22*, 1774.
(11) Bray, A. C.; Green, M.; Hankey, D. R.; Howard, J. A. K.; Johnson, O.; Stone, F. G. A. *J. Organomet. Chem.* **1985**, *281*, C12.
(12) (a) Vahrenkamp, H. *Adv. Organomet. Chem.* **1983**, *22*, 169. (b) Kaesz, H. D. In *Metal Clusters in Catalysis*; Knözinger, H., Gates, B. C., Guczi, L., Eds.; Elsevier: Amsterdam, 1986.
(13) Maclaughlin, S. A.; Taylor, N. J.; Carty, A. J. *Can. J. Chem.* **1982**, *60*, 87.

0020-1669/92/1331-4492$03.00/0 © 1992 American Chemical Society

cm × 5 cm (i.d.)) reaction vessel, the lamp being placed approximately 2 cm from the reaction solution. Chromatographic separation of the products was performed on silica gel TLC plates (20 cm × 20 cm; Merck, 2 mm). NMR spectra ($^{31}P\{^1H\}$, ^1H, and $^{13}C\{^1H\}$) were obtained on a Fourier-transform Bruker AC-200 or AM-250 spectrometer, using deuterated solvents as lock and reference (^1H and ^{13}C, $SiMe_4$ ($\delta = 0$); ^{31}P, 85% H_3PO_4 ($\delta = 0$)). Infrared spectra were recorded on a Nicolet 520 FTIR spectrometer as solutions in 0.5-mm matched sodium chloride cells. Microanalyses were performed by M-H-W Laboratories Phoenix, AZ. All chemicals, except where stated, were purchased from commercial sources and used as supplied. The starting material $Ru_4(CO)_{13}(\mu_3\text{-PPh})$ (**1**) was prepared from the pyrolysis of $(\mu\text{-H})Ru_3(CO)_{10}(\mu\text{-PPh}_2)$ as previously reported.[13,14]

Synthesis of $(\mu\text{-H})_2Ru_4(CO)_{12}(\mu_3\text{-PPh})$ (2). (a) Photochemical Process. A solution of **1** (203 mg, 0.232 μmol) in *n*-hexane (180 mL) was irradiated while a purge of dihydrogen was maintained through the solution. After 35 min of irradiation, the IR spectrum of the reaction solution indicated that almost all of the starting material had been consumed. During the course of the reaction, the color of the reaction solution changed from deep red to yellow. The solvent was removed in vacuo, the residue was dissolved in a minimum of benzene, and an equal volume of heptane was added. Cooling this solution to −10 °C in the presence of a seed crystal of $Ru_4(CO)_{13}(\mu_3\text{-PPh})$ (**1**) afforded a yellow-orange crystalline sample of $(\mu\text{-H})_2Ru_4(CO)_{12}(\mu_3\text{-PPh})$ (**2**). The supernatant liquid was filtered over cotton and the procedure of crystallization repeated to give a further crop of **2**. A total yield of 160 mg (81%) was obtained using this procedure.

(b) Thermal Route. Typically, a 200-mg sample of $Ru_4(CO)_{13}(\mu_3\text{-PPh})$ (**1**) was dissolved in 100 mL of *n*-hexane. A continuous hydrogen stream was bubbled through the solution, which was heated at 60 °C for 12 h, after which the IR spectrum indicated quantitative formation of **2**. The solution was cooled and the solvent removed under reduced pressure. The residue was extracted with CH_2Cl_2 and chromatographed on silica gel plates. Elution with dichloromethane/*n*-hexane (1/5, v/v) afforded a single major yellow band characterized spectroscopically as **2**. Crystallization as in part a afforded orange-yellow crystals of **2** in 70% yield. Anal. Calcd for $C_{18}H_7O_{12}PRu_4$ (MW 850.5): C, 25.42; H, 0.83; P, 3.64. Found: C, 25.69; H, 0.93; P, 3.79. IR (C_6H_{12}): ν(CO) 2099 w, 2073 vs, 2068 m, 2031 vs, 2024 m, 1970 w cm^{-1}. $^{31}P\{^1H\}$ NMR ($CDCl_3$, 294 K): δ 408 ppm. ^1H NMR (C_2D_6CO, 194 K): δ 7.41 (m, 5 H, C_6H_5), −19.3 ppm (d, J_{PH} = 16 Hz, 2 H, MHM). $^{13}C\{^1H\}$ NMR (CD_2Cl_2, 233 K): δ 200.2 (d, CO, $^2J_{PC}$ = 8.5 Hz), 199.2 (d, CO, $^2J_{PC}$ = 67 Hz), 196.1 (s, CO), 189.8 (s, CO), 187.5 (d, CO, $^2J_{PC}$ = 10.5 Hz), 185.6 (s, CO), 148.8–128.0 ppm (phenyl region).

Reaction of 2 with Cyclohexene and CO. A solution of **2** (102 mg, 0.12 μmol) and cyclohexene (0.5 mL) in heptane (250 mL) was irradiated with a continuous stream of CO gas passing through the solution. After 4 h of irradiation, the color of the reaction solution had changed from yellow to orange red. Formation of **1** was confirmed by monitoring the IR spectrum in the terminal carbonyl region during the course of the reaction. The solution was evaporated to dryness under reduced pressure and the residue chromatographed on silica gel plates. Elution with dichloromethane/hexane (1/5, v/v) allowed the separation of one major product, identified as **1**, and three minor products. The first minor band, obtainable only in trace quantities, was identified as $Ru_3(CO)_{12}$, and the next close running band corresponded to $(\mu\text{-H})_2Ru_3(CO)_9(\mu_3\text{-PPh})$.[15] Band 3 was characterized spectroscopically as **1** and was isolated as a red crystalline material upon crystallization from hexane/dichloromethane at −10 °C (0.064 g, 0.072 mmol) in 61% yield. Finally, a minor, slow-moving green band extracted from the plate was spectroscopically identified as the pentanuclear phosphinidene cluster $Ru_5(CO)_{15}(\mu_4\text{-PPh})$.[16] The identity of each of these products was confirmed by comparison of their spectroscopic properties with those already reported.

X-ray Structure Determination for 2. Crystallization from a mixture of benzene/hexane at −10 °C yielded dark red prisms of **2**. A crystal of approximate dimensions 0.20 (100) × 0.20 ($\bar{1}$00) × 0.17 (001) × 0.15 (011) × 0.15 (0$\bar{1}\bar{1}$) × 0.20 (01$\bar{1}$) mm (distances from common center) glued to a glass fiber using epoxy resin was mounted on a goniometer head and centered on an LT2-equipped Siemens R3m/v diffractometer. The unit cell parameters were determined and refined from a set of 25 general reflections ($22° < 2\theta < 32°$) well distributed in reciprocal space. Intensities were measured at −73 °C on a Siemens R3m/v diffractometer with the use of graphite-monochromated Mo Kα (λ = 0.710 73 Å) radiation. Data were collected through ω scans over the range $3.5° < 2\theta < 55°$ with variable scan speeds (2.93–29.30°/min) and a 1.2° scan width. Background measurements were made at the beginning and end of each scan, each for 25% of the total scan time. Two standard reflections monitored after every 100 intensity measurements showed no significant changes over the duration of the data collection. Data were corrected for Lorentz and polarization effects and absorption (face-indexed numerical). Of 10 620 data collected, 9482 ($F \geq 6.0\sigma(F)$) were considered observed and used in the structure solution and refinement.

Table I. Crystallographic Data for $(\mu\text{-H})_2Ru_4(CO)_{12}(\mu_3\text{-PPh})$ (**2**)

chem formula	$C_{18}H_7O_{12}PRu_4$	space group	$P\bar{1}$ (No. 2)
fw	850.5	T, °C	−73
a, Å	10.059 (2)	λ (Mo Kα), Å	0.710 73
b, Å	13.678 (3)	ρ_{calcd}, g cm^{-3}	2.319
c, Å	18.093 (5)	μ, cm^{-1}	25.11
α, deg	85.60 (2)	min–max transm coeff	0.4356–0.5521
β, deg	78.97 (2)		
γ, deg	88.65 (2)	R,[a] %	2.77
V, Å^3	2436.2 (10)	R_w,[b] %	3.44
Z	4		

[a] $R = \Sigma||F_o| - |F_c||/\Sigma|F_o|$. [b] $R_w = [\Sigma w(|F_o| - |F_c|)^2/\Sigma wF_o^2)]^{1/2}$.

A Patterson synthesis readily yielded the positions of the metal atoms. Standard Fourier methods were used to locate the remaining atoms in the molecule. All calculations were performed using SHELXTL PLUS software. Full-matrix least-squares refinement of positional and isotropic thermal parameters, subsequent conversion to anisotropic coefficients for all non-hydrogen atoms, and several further cycles of refinement gave R = 3.23%. At this stage, a difference Fourier map revealed the positions of all the hydrogen atoms. In the final cycles of refinement, hydrogen atoms of the phenyl ring were included as riding on their respective carbon atoms and the hydride ligands were fixed in their found positions. Convergence was reached at R = 2.77% and R_w = 3.44%. The function minimized in the least-squares calculations was $\Sigma w|F_o - F_c|^2$. In the final cycles, an empirical weighting scheme of the form $w^{-1} = \sigma^2(F)$ was employed. A final difference Fourier map exhibited maximum and minimum residues of 0.78 and −0.66 e Å^{-3}, respectively, in the vicinity of the ruthenium atoms. The atomic scattering factors used, including anomalous dispersion corrections for ruthenium, were taken from ref 17; for hydrogen, those of Stewart et al. were employed.[18] Crystallographic data and details of the data collection are given in Table I; atomic coordinates are listed in Table II. Tables III and IV contain appropriate selections of bond lengths and angles.

Results

The photochemical reaction of dihydrogen with the butterfly cluster **1** proceeds rapidly (35 min) at room temperature, forming $(\mu\text{-H})_2Ru_4(CO)_{12}(\mu_3\text{-PPh})$ (**2**) in quantitative yield. Remarkably, there are still very few examples of facile activation of dihydrogen by transition metal clusters, and in the majority of cases where such facile processes have been observed, unsaturated clusters have been involved.[19] The quantitative formation of **2** was confirmed by analyzing the terminal carbonyl stretching region of the IR spectrum. The reaction was accompanied by a dramatic color change from deep red to yellow.

The presence of metal–hydride bonding in **2** was established using ^1H NMR spectroscopy, a high-field doublet resonance at δ −19.3 ppm (J_{PH} = 16.0 Hz) being typical of a bridging hydride. The $^{31}P\{^1H\}$ NMR spectrum consisted of a singlet resonance at δ 408 ppm, very close to the value found for the phosphorus signal of the precursor **1** (δ = 409 ppm), implying that the structural integrity of the cluster had been retained. These shifts are within

(14) Van Gastel, F.; Taylor, N. J.; Carty, A. J. *Inorg. Chem.* **1989**, *28*, 384.
(15) Iwasaki, F.; Mays, M. J.; Raithby, P. R.; Taylor, P. L.; Wheatley, P. J. *J. Organomet. Chem.* **1981**, *213*, 185.
(16) Natarajan, K.; Zsolnai, L.; Hüttner, G. *J. Organomet. Chem.* **1981**, *209*, 85.
(17) *International Tables for X-ray Crystallography*; Kynoch Press: Birmingham, England, 1974; Vol. 4.
(18) Stewart, R. F.; Davidson, E. R.; Simpson, W. T. *J. Chem. Phys.* **1965**, *42*, 3175.
(19) (a) Adams, R. D.; Wang, S. *Organometallics* **1986**, *5*, 1272. (b) Burch, R. R.; Schusterman, A. J.; Muetterties, E. L.; Teller, R. J.; Williams, J. M. *J. Am. Chem. Soc.* **1983**, *105*, 3546.

Table II. Atomic Coordinates (× 10^4) for $(\mu\text{-H})_2Ru_4(CO)_{12}(\mu_3\text{-PPh})$ (**2**) and Equivalent Isotropic Displacement Coefficients (Å² × 10^3)

atom	x	y	z	U(eq)[a]	atom	x	y	z	U(eq)[a]
				Molecule A					
Ru(1)	792.7 (3)	2431.9 (3)	5002.4 (2)	27.7 (1)	C(2)	1486 (5)	1349 (4)	4386 (3)	42 (2)
Ru(2)	776.7 (3)	1715.2 (2)	6535.0 (2)	24.5 (1)	C(3)	−1061 (5)	2075 (4)	5066 (3)	38 (2)
Ru(3)	3292.3 (3)	2388.4 (3)	5687.9 (2)	27.1 (1)	C(4)	933 (5)	487 (4)	6098 (3)	44 (2)
Ru(4)	1635.8 (3)	3601.3 (2)	6848.7 (2)	23.8 (1)	C(5)	1676 (5)	1322 (3)	7347 (3)	36 (2)
P(1)	152.6 (11)	3287.1 (8)	6064.2 (6)	24.8 (3)	C(6)	−1041 (5)	1448 (3)	7021 (3)	32 (1)
O(1)	879 (4)	3847 (3)	3611 (2)	60 (2)	C(7)	4788 (5)	3018 (4)	5003 (3)	39 (2)
O(2)	1862 (4)	740 (3)	4005 (2)	64 (2)	C(8)	3562 (5)	1119 (4)	5308 (3)	41 (2)
O(3)	−2167 (4)	1882 (3)	5143 (2)	57 (2)	C(9)	4420 (5)	2029 (4)	6397 (3)	37 (2)
O(4)	997 (5)	−276 (3)	5882 (3)	71 (2)	C(10)	2872 (5)	3268 (3)	7546 (3)	32 (1)
O(5)	2241 (4)	1044 (3)	7821 (2)	50 (1)	C(11)	1960 (5)	4973 (3)	6689 (3)	35 (2)
O(6)	−2128 (4)	1246 (3)	7306 (2)	51 (1)	C(12)	254 (5)	3782 (3)	7711 (3)	35 (2)
O(7)	5666 (4)	3358 (3)	4588 (2)	54 (1)	C(13)	−1572 (4)	3795 (3)	6230 (3)	31 (1)
O(8)	3740 (4)	361 (3)	5084 (2)	55 (2)	C(14)	−1995 (5)	4316 (3)	5625 (3)	41 (2)
O(9)	5136 (4)	1814 (3)	6803 (2)	50 (1)	C(15)	−3242 (6)	4780 (4)	5723 (4)	53 (2)
O(10)	3517 (4)	3065 (3)	7984 (2)	45 (1)	C(16)	−4077 (5)	4738 (4)	6428 (4)	59 (2)
O(11)	2135 (4)	5795 (3)	6607 (2)	57 (2)	C(17)	−3673 (5)	4223 (4)	7033 (4)	51 (2)
O(12)	−497 (4)	3882 (3)	8250 (2)	60 (2)	C(18)	−2404 (5)	3773 (4)	6933 (3)	41 (2)
C(1)	854 (5)	3330 (4)	4140 (3)	39 (2)					
				Molecule B					
Ru(1)	5116.6 (3)	9058.5 (2)	8110.3 (2)	24.5 (1)	C(2)	4963 (5)	9440 (3)	7070 (3)	38 (2)
Ru(2)	4860.6 (4)	6969.3 (2)	8312.0 (2)	26.3 (1)	C(3)	7048 (5)	8972 (4)	7857 (3)	37 (2)
Ru(3)	2413.9 (3)	8055.0 (3)	8379.2 (2)	25.9 (1)	C(4)	5449 (5)	7195 (3)	7250 (3)	39 (2)
Ru(4)	3286.5 (4)	7184.3 (3)	9797.2 (2)	28.3 (1)	C(5)	3759 (5)	5847 (3)	8316 (3)	36 (2)
P(1)	5139.8 (11)	8089.6 (8)	9201.8 (6)	25.1 (3)	C(6)	6460 (5)	6241 (4)	8430 (3)	42 (2)
O(1)	5098 (4)	11148 (3)	8583 (2)	46 (1)	C(7)	948 (5)	9012 (3)	8527 (3)	33 (1)
O(2)	4876 (5)	9681 (3)	6466 (2)	64 (2)	C(8)	2617 (5)	8085 (4)	7305 (3)	39 (2)
O(3)	8197 (4)	8886 (3)	7712 (2)	56 (2)	C(9)	1198 (5)	6989 (4)	8461 (3)	40 (2)
O(4)	5850 (5)	7274 (3)	6613 (2)	60 (2)	C(10)	2007 (5)	6098 (4)	9911 (3)	43 (2)
O(5)	3147 (4)	5163 (3)	8300 (2)	54 (2)	C(11)	2456 (5)	7884 (4)	10637 (3)	41 (2)
O(6)	7394 (4)	5772 (3)	8476 (3)	70 (2)	C(12)	4343 (6)	6393 (4)	10369 (3)	49 (2)
O(7)	127 (3)	9577 (3)	8591 (2)	47 (1)	C(13)	6621 (4)	8187 (3)	9642 (2)	31 (1)
O(8)	2670 (4)	8088 (3)	6674 (2)	58 (2)	C(14)	6959 (5)	9123 (4)	9798 (3)	41 (2)
O(9)	443 (4)	6372 (3)	8493 (3)	63 (2)	C(15)	8040 (6)	9256 (5)	10162 (3)	57 (2)
O(10)	1332 (5)	5431 (3)	9988 (3)	70 (2)	C(16)	8756 (5)	8454 (6)	10384 (3)	61 (3)
O(11)	1944 (4)	8310 (4)	11127 (2)	67 (2)	C(17)	8459 (6)	7547 (5)	10226 (3)	60 (2)
O(12)	4940 (5)	5909 (3)	10729 (3)	81 (2)	C(18)	7378 (5)	7393 (4)	9859 (3)	46 (2)
C(1)	5077 (5)	10372 (3)	8404 (2)	33 (1)					

[a] $U(\text{eq}) = (1/3)\sum_i\sum_j U_{ij}a_i^*a_j^*a_i\cdot a_j$.

Table III. Selected Bond Lengths (Å) for $(\mu\text{-H})_2Ru_4(CO)_{12}(\mu_3\text{-PPh})$ (**2**)

	molecule A	molecule B		molecule A	molecule B
Ru(1)–Ru(2)	2.866 (1)	2.864 (1)	Ru(3)–C(7)	1.930 (5)	1.942 (5)
Ru(1)–Ru(3)	3.006 (1)	3.013 (1)	Ru(3)–C(8)	1.911 (6)	1.913 (5)
Ru(2)–Ru(3)	2.830 (1)	2.832 (1)	Ru(3)–C(9)	1.899 (5)	1.904 (5)
Ru(2)–Ru(4)	2.871 (1)	2.879 (1)	Ru(4)–C(10)	1.957 (5)	1.962 (6)
Ru(3)–Ru(4)	3.001 (1)	3.019 (1)	Ru(4)–C(11)	1.903 (5)	1.904 (6)
Ru(1)–P(1)	2.304 (1)	2.296 (1)	Ru(4)–C(12)	1.908 (4)	1.888 (6)
Ru(2)–P(1)	2.367 (1)	2.364 (1)	C(1)–O(1)	1.144 (6)	1.136 (6)
Ru(4)–P(1)	2.315 (1)	2.303 (1)	C(2)–O(2)	1.134 (7)	1.136 (6)
Ru(1)–H(1)	1.57	1.51	C(3)–O(3)	1.129 (6)	1.140 (6)
Ru(3)–H(1)	1.74	1.93	C(4)–O(4)	1.138 (7)	1.145 (6)
Ru(3)–H(2)	1.95	1.75	C(5)–O(5)	1.152 (7)	1.137 (6)
Ru(4)–H(2)	1.51	1.74	C(6)–O(6)	1.146 (6)	1.138 (7)
Ru(1)–C(1)	1.902 (5)	1.909 (5)	C(7)–O(7)	1.127 (6)	1.113 (6)
Ru(1)–C(2)	1.958 (5)	1.948 (5)	C(8)–O(8)	1.140 (7)	1.132 (6)
Ru(1)–C(3)	1.919 (5)	1.912 (5)	C(9)–O(9)	1.142 (7)	1.140 (7)
Ru(2)–C(4)	1.902 (5)	1.902 (5)	C(10)–O(10)	1.131 (6)	1.135 (7)
Ru(2)–C(5)	1.906 (5)	1.913 (5)	C(11)–O(11)	1.135 (6)	1.131 (7)
Ru(2)–C(6)	1.902 (4)	1.910 (5)	C(12)–O(12)	1.129 (6)	1.135 (8)

the normal range for μ_3- and μ_4-phenylphosphinidene ligands in electron-precise Ru_4 and Ru_5 clusters.[20] On the basis of microanalytical and spectroscopic data, we tentatively assigned the formulation $(\mu\text{-H})_2Ru_4(CO)_{12}(\mu_3\text{-PPh})$ to the product. The appearance of a single high-field doublet in the ^{1}H NMR spectrum indicates the presence of two chemically equivalent hydride ligands coupled to a single phosphorus atom. These hydrides are therefore most likely located at the ruthenium–ruthenium bonds in the Ru_3P base of the square pyramid. In order to confirm the postulated retention of the butterfly core geometry and the location of the bridging hydride ligands, crystals of **2** were grown from a benzene/heptane solution at −10 °C. Compound **2** is quite unstable in solution, as it decomposed to $(\mu\text{-H})_2Ru_3(CO)_9(\mu_3\text{-PPh})$ quickly enough that it was necessary to seed the crystallization of **2** with a crystal of the precursor **1**. Greater stability in solution is observed under an atmosphere of dihydrogen, and in the solid state $(\mu\text{-H})_2Ru_4(CO)_{12}(\mu_3\text{-PPh})$ shows little tendency to fragment, as it can be kept for several months without significant decomposition.

Compound **2** crystallizes with two independent but essentially identical molecules in each asymmetric unit of the triclinic unit cell. The molecular structure of one of these molecules (molecule A) is shown in Figure 1. As anticipated, the skeletal framework has been retained upon hydrogenation. The four ruthenium atoms adopt a butterfly skeletal arrangement with the phosphinidene ligand capping the open Ru_3 triangle composed of the two wingtip metals Ru(1) and Ru(4) and the hinge atom Ru(2). The four atoms Ru(1), Ru(3), Ru(4), and P(1) lie almost in a plane, with the greatest deviation from a best least-squares plane being for P(1) (−0.028 Å in molecule A; −0.051 Å in molecule B).[21] The hydride ligands were located crystallographically as bridging the two hinge to wingtip Ru(3)–Ru(1) and Ru(3)–Ru(4) edges. In both molecules, they lie slightly below the base of the square

(20) (a) Carty, A. J.; Maclaughlin, S. A.; Nucciarone, D. in *Phosphorus-31 NMR Spectroscopy in Stereochemical Analysis: Organic Compounds and Metal Complexes*; Verkade, J. G., Quinn, L. D., Eds.; VCH Publishers: New York, 1987; Chapter 16, p 605. (b) Liddell, M. J. Ph.D. Thesis, University of Adelaide, 1989. (c) Knox, S. A. R.; Lloyd, B. R.; Orpen, A. G.; Vinas, J. M.; Weber, M. J. *J. Chem. Soc., Chem. Commun.* **1987**, 1487.

(21) The deviations of atoms Ru(1), Ru(3), Ru(4), and P(1) from a least-squares plane are respectively as follows. Molecule A: +0.021, +0.021, −0.014, −0.028 Å. Molecule B: +0.038, +0.038, −0.025, −0.051 Å.

Table IV. Selected Bond Angles (deg) for $(\mu\text{-H})_2Ru_4(CO)_{12}(\mu_3\text{-PPh})$ (**2**)

	molecule A	molecule B
Ru(2)-Ru(1)-Ru(3)	57.6 (1)	57.5 (1)
Ru(2)-Ru(1)-P(1)	53.1 (1)	53.2 (1)
Ru(3)-Ru(1)-P(1)	76.3 (1)	77.3 (1)
Ru(2)-Ru(1)-C(1)	159.8 (2)	157.0 (1)
Ru(3)-Ru(1)-C(1)	114.7 (2)	115.6 (1)
P(1)-Ru(1)-C(1)	108.1 (2)	104.9 (1)
Ru(2)-Ru(1)-C(2)	105.8 (2)	106.9 (1)
Ru(3)-Ru(1)-C(2)	91.3 (2)	90.6 (2)
P(1)-Ru(1)-C(2)	158.9 (2)	160.0 (1)
Ru(2)-Ru(1)-C(3)	92.4 (2)	92.2 (1)
Ru(3)-Ru(1)-C(3)	149.7 (2)	148.9 (2)
P(1)-Ru(1)-C(3)	89.4 (2)	90.0 (1)
Ru(1)-Ru(2)-Ru(3)	63.7 (1)	63.9 (1)
Ru(1)-Ru(2)-Ru(4)	89.8 (1)	88.8 (1)
Ru(3)-Ru(2)-Ru(4)	63.5 (1)	63.8 (1)
Ru(1)-Ru(2)-P(1)	51.2 (1)	51.0 (1)
Ru(3)-Ru(2)-P(1)	79.1 (1)	80.1 (1)
Ru(4)-Ru(2)-P(1)	51.4 (1)	51.0 (1)
Ru(1)-Ru(2)-C(4)	81.9 (2)	77.1 (1)
Ru(3)-Ru(2)-C(4)	93.4 (2)	95.6 (2)
Ru(4)-Ru(2)-C(4)	156.7 (2)	158.9 (2)
P(1)-Ru(2)-C(4)	131.0 (2)	124.3 (2)
Ru(1)-Ru(2)-C(5)	151.9 (1)	147.8 (1)
Ru(3)-Ru(2)-C(5)	88.5 (1)	85.2 (1)
Ru(4)-Ru(2)-C(5)	80.8 (1)	85.0 (1)
P(1)-Ru(2)-C(5)	131.2 (1)	135.6 (1)
Ru(1)-Ru(2)-C(6)	108.7 (1)	116.4 (2)
Ru(3)-Ru(2)-C(6)	170.3 (1)	171.3 (2)
Ru(4)-Ru(2)-C(6)	111.9 (1)	107.5 (2)
P(1)-Ru(2)-C(6)	91.4 (1)	93.4 (2)
Ru(1)-Ru(3)-Ru(2)	58.7 (1)	58.6 (1)
Ru(1)-Ru(3)-Ru(4)	84.8 (1)	83.5 (1)
Ru(2)-Ru(3)-Ru(4)	58.9 (1)	58.8 (1)
Ru(1)-Ru(3)-C(7)	111.1 (2)	110.5 (1)
Ru(2)-Ru(3)-C(7)	168.5 (2)	167.1 (2)
Ru(4)-Ru(3)-C(7)	117.5 (2)	115.7 (1)
Ru(1)-Ru(3)-C(8)	84.0 (2)	86.7 (2)
Ru(2)-Ru(3)-C(8)	87.7 (1)	90.3 (2)
Ru(4)-Ru(2)-C(8)	145.7 (1)	148.1 (2)
Ru(1)-Ru(3)-C(9)	157.5 (1)	156.7 (2)
Ru(2)-Ru(3)-C(9)	99.5 (1)	98.6 (2)
Ru(4)-Ru(3)-C(9)	88.1 (1)	88.3 (2)
Ru(2)-Ru(4)-Ru(3)	57.6 (1)	57.3 (1)
Ru(2)-Ru(4)-P(1)	53.0 (1)	52.9 (1)
Ru(3)-Ru(4)-P(1)	76.3 (1)	77.1 (1)
Ru(2)-Ru(4)-C(10)	102.9 (1)	102.0 (2)
Ru(3)-Ru(4)-C(10)	90.7 (1)	92.6 (2)
P(1)-Ru(4)-C(10)	155.9 (1)	154.6 (2)
Ru(2)-Ru(4)-C(11)	157.0 (2)	155.6 (2)
Ru(3)-Ru(4)-C(11)	114.8 (1)	110.0 (2)
P(1)-Ru(4)-C(11)	105.2 (2)	106.0 (2)
Ru(2)-Ru(4)-C(12)	97.0 (1)	99.1 (2)
Ru(3)-Ru(4)-C(12)	153.4 (1)	156.1 (2)
P(1)-Ru(4)-C(12)	95.0 (2)	92.0 (2)
Ru(1)-P(1)-Ru(2)	75.7 (1)	75.8 (1)
Ru(1)-P(1)-Ru(4)	122.5 (1)	121.8 (1)
Ru(2)-P(1)-Ru(4)	75.6 (1)	76.1 (1)
Ru(1)-H(1)-Ru(3)	131	122
Ru(3)-H(2)-Ru(4)	120	120

pyramid.[22] Table VI shows a comparison of the skeletal core between the precursor **1** and compound **2**. Ignoring the hydride positions, the pseudomirror plane passing through P(1), Ru(2), and Ru(3) in **1**[13] is retained in **2**. The proton NMR spectrum of **2** is virtually invariant over the temperature range 298–200 K, with a single doublet ($\delta = -19.3$ ppm; $J_{PH} = 16$ Hz) being consistent with the equivalent hydride ligands. A similar observation has been made for $H_2Os_4(CO)_{12}(\mu_3\text{-PPh})$.[23] The dihedral angle between the wings of the butterfly of 104° (102.4° for molecule B) is much smaller than found in cluster **1** (111.2°) but is accompanied by a lengthening of the nonbonding Ru(1)–Ru(4) distance (4.051 (1) and 4.018 (1) Å for molecules A and B, respectively, versus 4.012 (1) Å for **1**). Smaller values of dihedral angles have similarly been observed in butterfly clusters containing hydride ligands bridging hinge to wingtip edges.[24] In these cases, the amplitude of the dihedral angle is probably a consequence of constraints brought about by the position of the bridging hydride ligands rather than by an electronic requirement of the bonding within the cluster core. The same interpretation could be given for the larger Ru(1)–Ru(4) separation in **2**, which may be viewed as a side effect of the frequently observed lengthening of unsupported metal–metal bonds produced by bridging hydrides.[25]

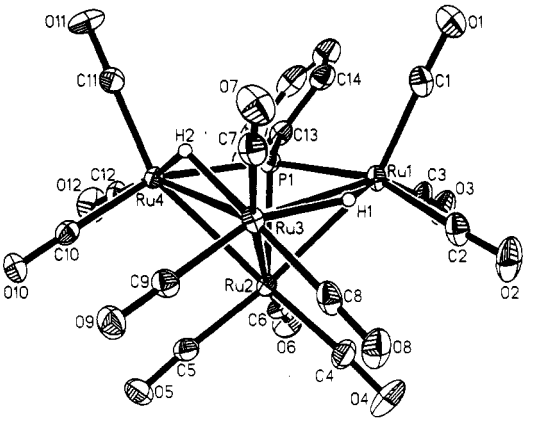

Figure 1. Molecular structure of one of the independent molecules of $(\mu\text{-H})_2Ru_4(CO)_{12}(\mu_3\text{-PPh})$ (**2**). Thermal ellipsoids are drawn at the 50% probability level.

Analysis of the metal–metal bond distances in **2** shows that the presence of two hydride-bridged Ru–Ru bonds has substantially altered the core geometry of $Ru_4(CO)_{13}(\mu_3\text{-PPh})$. The longest metal–metal bonds correspond to the hydride hinge–wingtip edges Ru(3)–Ru(1) (3.006 (1) Å for molecule A; 3.013 (1) Å for molecule B) and Ru(3)–Ru(4) (3.001 (1) Å for molecule A; 3.019 (1) Å for molecule B). These distances compare favorably with the values of 3.009 (1) and 3.021 (1) Å found in $(\mu\text{-H})_3Ru_4(CO)_{12}(\mu_2\text{-NCO})$,[10] where the isocyanate group bridges the wingtip metals, but are significantly longer than the bond lengths of 2.783 (1) and 2.789 (1) Å observed in $(\mu\text{-H})_3Ru_4(CO)_{11}(\mu_4\text{-N})$.[26] In this case, the expansion of the metal framework is limited by the bonding requirements of the nitride ligand, which caps all four metal atoms. For comparison, the hydride-bridged metal distances in tetrahedral Ru_4 clusters lie in an intermediate range of values between 2.892 (1) and 2.959 (1) Å (Table V). The shortest metal–metal bond is the hinge bond Ru(2)–Ru(3) of 2.830 (1) Å (2.832 (1) Å for molecule B), which is considerably shorter than in compound **1** (average of 0.143 Å for the two molecules). The phosphinidene-capped hinge–wingtip edge

(22) Hydrogen atoms H(1) and H(2) lie respectively +0.11 and +0.85 Å (molecule A) and +0.77 and +0.82 Å (molecule B) above the plane defined in ref 21.

(23) Colbran, J. B.; Johnson, B. F. G.; Lahoz, F. J.; Lewis, J.; Raithby, P. R. *J. Chem. Soc., Dalton Trans.* **1988**, 1199.
(24) Sappa, E.; Tiripicchio, A.; Carty, A. J.; Toogood, G. E. *Prog. Inorg. Chem.* **1987**, *35*, 437.
(25) Teller, R. G.; Bau, R. *Struct. Bonding (Berlin)* **1981**, *44*, 1.
(26) Collins, M. A.; Johnson, B. F. G.; Lewis, J.; Mace, J. M.; Morris, J.; McPartlin, M.; Nelson, W. J. H.; Puga, J.; Raithby, P. R. *J. Chem. Soc., Chem. Commun.* **1983**, 689.
(27) Steinmetz, G. R.; Harley, A. D.; Geoffroy, G. L. *Inorg. Chem.* **1980**, *19*, 2985.
(28) Braga, D.; Johnson, B. F. G.; Lewis, J.; Mace, J. M.; McPartlin, M.; Puga, J.; Nelson, W. J. H.; Raithby, P. R.; Whitmire, K. H. *J. Chem. Soc., Chem. Commun.* **1982**, 1081.
(29) Harris, S.; Blohm, M. L.; Gladfelter, W. L. *Inorg. Chem.* **1989**, *28*, 2290.
(30) Yawney, D. B. W.; Doedens, R. J. *Inorg. Chem.* **1972**, *11*, 838.
(31) Jones, P. G. *Acta Crystallogr.* **1989**, *C45*, 1077.
(32) McPartlin, M.; Nelson, W. J. H. *J. Chem. Soc., Dalton Trans.* **1986**, 1557.
(33) Wilson, R. D.; Wu, S. M.; Love, R. A.; Bau, R. *Inorg. Chem.* **1978**, *17*, 1271.

Table V. M–M Bond Lengths (Å) in Tetranuclear Ruthenium Hydride Clusters and Related Molecules

compound	Ru–Ru	electron count	geometry	ref
$(PPN)Ru_4(CO)_{13}(\mu\text{-Cl})$	2.797 (1), 2.813 (1), 2.814 (1), 2.791 (1), 2.832 (1)[d]	62	butterfly	27
$H_3Ru_4(CO)_{12}(\mu\text{-NCO})$	2.823 (1), 2.825 (1), 3.009 (1),[b] 3.021 (1),[b] 2.949 (1)[b,d]	62	butterfly	10
$Ru_4(CO)_{13}(\mu_3\text{-PPh})$	2.9735 (10),[d] 2.8332 (9), 2.7844 (9), 2.8612 (9), 2.9241 (10)	62	butterfly	13
$H_2Ru_4(CO)_{12}(\mu_3\text{-PPh})$[a]	2.830 (1),[d] 2.866 (1), 2.871 (1), 3.006 (1),[b] 3.001 91)[b] 2.832 (1),[d] 2.864 (1), 2.879 (1), 3.013 (1),[b] 3.019 (1)[b]	62	butterfly	this work
$H_3Ru_4(CO)_{11}(\mu_4\text{-N})$[a]	2.783 (1),[b] 2.794 (1), 2.811 (1),[b,d] 2.794 (1),[b] 2.798 (1) 2.794 (1),[b] 2.789 (1), 2.810 (1), 2.797 (1),[b] 2.790 (1)	62	butterfly	26
$HRu_4(CO)_{11}(\mu_4\text{-N})[P(OMe)_3]$	2.832 (1), 2.801 (1), 2.773 (1), 2.770 (1), 2.804 (1)[b,d]	62	butterfly	28
$(PPN)Ru_4(CO)_{12}(\mu_4\text{-N})$	2.672 (1),[d] 2.779 (1), 2.798 (1), 2.789 (1), 2.781 (1), 2.781 (1)	62	butterfly	29
$H_2Ru_4(CO)_{13}$[a]	2.785 (7), 2.915 (7),[b] 2.947 (6),[b] 2.764 (7),[c] 2.762 (6),[c] 2.818 (7) 2.771 (7), 2.924 (7),[b] 2.935 (8),[b] 2.787 (7),[c] 2.778 (7),[c] 2.805 (8)	60	tetrahedral	30
$(PPN)H_3Ru_4(CO)_{12}$[d]	2.915 (1),[b] 2.796 (1), 2.955 (1),[b] 2.773 (1), 2.799 (1), 2.921 (1)[b]	60	tetrahedron	31
	2.959 (1),[b] 2.799 (1), 2.892 (1),[b] 2.916 (1),[b] 2.803 (1), 2.805 (1)	60	tetrahedral	32
	2.935 (1),[b] 2.799 (1), 2.941 (1),[b] 2.777 (1), 2.936 (1),[b] 2.786 (1)	60	tetrahedral	32
$H_4Ru_4(CO)_{12}$	2.7839 (8), 2.9502 (9),[b] 2.9446 (8),[b] 2.9483 (8),[b] 2.9565 (7),[b] 2.7881 (8)	60	tetrahedral	33

[a] Values for two independent molecules given. [b] H-bridged. [c] CO bridged. [d] Values for isomers given. [e] Hinge of the butterfly.

Table VI. Modification of the Skeletal Core of $Ru_4(CO)_{13}(\mu_3\text{-PPh})$ (**1**) upon Hydrogenation

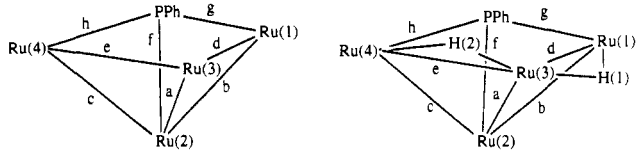

	$Ru_4(CO)_{13}(\mu_3\text{-PPh})$ (**1**)	$(\mu\text{-H})_2Ru_4(CO)_{12}(\mu_3\text{-PPh})$ (**2**)	
		molecule A	molecule B
bond dist, Å			
a	2.9735 (10)	2.830 (1)	2.832 (1)
b	2.8332 (9)	2.866 (1)	2.864 (1)
c	2.7844 (9)	2.871 (1)	2.879 (1)
d	2.8612 (9)	3.006 (1)	3.013 (1)
e	2.9241 (10)	3.001 (1)	3.019 (1)
f	2.388 (2)	2.367 (1)	2.364 (1)
g	2.302 (2)	2.304 (1)	2.299 (1)
h	2.316 (2)	2.315 (1)	2.303 (1)
nonbonding Ru···Ru, Å	4.012	4.051 (1)	4.018 (1)
nonbonding Ru···P, Å	3.199	3.325 (1)	3.364 (1)
dihedral angle, deg	111.2	104	102.4

lengths Ru(2)–Ru(1) of 2.866 (1) Å and Ru(2)–Ru(4) of 2.871 (1) Å (2.864 (1) and 2.879 (1) Å for molecule B) are also slightly longer than found in **1**.

The trend in Ru–P distances in **2** is essentially similar to that of **1**, the hinge Ru–P bond length (average of 2.366 Å for the two molecules) being longer than the wingtip Ru–P distances (average of 2.305 Å). The Ru–P bond lengths in **2** lie within the range of values found in ruthenium clusters where a phosphinidene ligand caps an open Ru_3 triangular face (2.302–2.395 Å),[13,34] which are slightly longer than the values found in systems where a phosphinidene caps a closed triangular face (2.275–2.329 Å).[15,35] The low-temperature X-ray structural analysis, which allowed the unequivocal location of the hydride ligands, reveals some interesting features. In molecule A, the hydride ligands asymmetrically bridge the hinge to wingtip edges, the hydrogen atoms being more strongly bonded to the wingtip metal atoms (Ru(1)–H(1) = 1.57 Å and Ru(4)–H(2) = 1.51 Å) than to the hinge ruthenium atom (Ru(3)–H(1) = 1.74 Å and Ru(3)–H(2) = 1.95 Å). In molecule B, the Ru(1)–Ru(3) vector is unevenly spanned by the hydride ligand (Ru(1)–H(1) = 1.51 Å and Ru(3)–H(1) = 1.93 Å) whereas the Ru(4)–Ru(3) edge is uniformly bridged (Ru(4)–H(2) = 1.74 Å and Ru(3)–H(2) = 1.75 Å). Since the hydrogen atom positions were not refined however, further comment on the apparent differences in Ru–H bond lengths is not justified. The compound $(\mu\text{-H})_2Os_4(CO)_{12}(\mu_3\text{-}PC_6H_{11})$ presents structural features analogous to those of **2** but exhibits a greater thermal stability, as it was isolated from the reaction of $(\mu\text{-H})_2Os_3(CO)_9(\mu_3\text{-}PC_6H_{11})$ with $Os_3(CO)_{12}$ in refluxing nonane.[23]

All attempts to reductively eliminate dihydrogen from **2** failed, resulting only in cluster fragmentation. Photolysis of a heptane solution of **2** with a continuous CO purge gave nearly quantitative conversion to the trinuclear phosphinidene-stabilized cluster $(\mu\text{-H})_2Ru_3(CO)_9(\mu_3\text{-PPh})$. This cluster degradation can be suppressed by addition of an excess of cyclohexene, the conversion of **2** back to **1** in high yields (61%) occurring through reduction of the olefin.

A number of examples of addition of dihydrogen to metal clusters have been reported.[1] In electron-precise clusters, reaction with H_2 appears to be preceded by formation of a vacant coordination site through the loss of a carbonyl ligand. Kinetic studies of the reversible hydrogenation of $HRu_3(CO)_{10}(\mu\text{-COMe})$ showed that dissociation of CO occurs prior to the rate-determining step, which is thought to be the oxidative addition of molecular hydrogen.[8] However, it has also been suggested that homolysis of a metal–metal bond may be an important step in the photoinitiated reaction of H_2 with certain metal carbonyl clusters.[4] Recently, reversible addition of dihydrogen to a metal cluster resulting in concomitant metal–metal bond scission/formation has been reported. The closed 48-electron $(\mu\text{-H})_2Ru_3(CO)_8(\mu\text{-Bu}^t_2P)_2$ complex readily adds H_2 at ambient temperature without CO loss to yield $(\mu\text{-H})_2(H)_2Ru_3(CO)_8(\mu\text{-Bu}^t_2P)_2$.[9] The latter rapidly loses H_2 in solution when exposed to a nitrogen purge or vacuum. X-ray crystallographic analysis of both compounds indicates that H_2 addition occurs through rupture of the unbridged Ru–Ru edge, which is re-formed upon H_2 elimination. An alternative route of hydrogen activation without metal–metal bond scission or CO loss was recently observed. The reaction of $Ru_3(CO)_8[(\mu_3\text{-PPh})(C_5H_4N)](\mu\text{-PPh}_2)$ with H_2 at 80 °C leads to the formation of $Ru_3(CO)_8[(\mu_3\text{-PPh})(C_5H_4N)](PPh_2H)$,[36] among other products. In this case, the creation of a vacant coordination site is provided by lowering the hapticity of a bridging ligand, and hydrogen activation results in the formation of a bridging hydride and the conversion of a phosphido bridge to a phosphine ligand. The reaction is quasi-reversible, as heating at 80 °C under an inert atmosphere quantitatively leads to re-formation of the precursor.

For tetranuclear systems, modification of the cluster frame appears to accompany activation of molecular hydrogen in most

(34) Field, J. S.; Haines, R. J.; Smit, D. N. *J. Organomet. Chem.* **1982**, *240*, C23.

(35) (a) Natarajan, K.; Scheidsteger, O.; Hüttner, G. *J. Organomet. Chem.* **1981**, *221*, 301. (b) Bruce, M. I.; Horn, E.; Shawkataly, O. B.; Snow, M. R.; Tiekink, E. R. J.; Williams, M. L. *J. Organomet. Chem.* **1986**, *316*, 187.

(36) Lugan, N.; Lavigne, G.; Bonnet, J. J.; Reau, R.; Neibecker, D.; Tkatchenko, I. *J. Am. Chem. Soc.* **1988**, *110*, 5369.

cases. The addition of dihydrogen to the tetrahedral sulfido cluster $Os_4(CO)_{12}(\mu_3\text{-}S)$ at high temperature proceeds without CO loss but with scission of one metal–metal bond to yield the butterfly $(\mu\text{-}H)_2Os_4(CO)_{12}(\mu_3\text{-}S)$, which is isostructural with **2**.[37] Dihydrogen addition to the 64-electron butterfly cluster $Os_4(CO)_{12}(\mu_3\text{-}S)_2$ surprisingly results in the electron-precise cluster $(\mu\text{-}H)_2Os_4(CO)_{12}(\mu_3\text{-}S)_2$ without the elimination of carbonyl ligands.[38] The latter possesses a trigonal prismatic skeletal framework with only three metal–metal bonds, the hydrides bridging an Os–Os edge of each of the triangular faces. Unexpectedly, hydrogenation of the planar 64-electron butterfly cluster $Ru_4(CO)_{13}(\mu\text{-}PPh_2)_2$ leads to metal–metal bond formation.[7b] Activation of dihydrogen occurs with dissociation of three carbonyl ligands and transformation of the planar butterfly to a tetrahedral cluster. Upon addition of carbon monoxide, the butterfly geometry is restored with elimination of H_2.

For $Ru_4(CO)_{13}(\mu_3\text{-}PPh)$, hydrogenation occurs with CO loss but retention of the skeletal configuration. The compound does react with H_2 at ambient temperature, but the longer rection time required for complete conversion leads to fragmentation of **2**.[39] Attempts to generate the closed trigonal bipyramidal cluster $Ru_4(CO)_{12}(\mu_3\text{-}PPh)$ via irradiation of **1** in heptane failed, the condensation products $Ru_5(CO)_{15}(\mu_4\text{-}PPh)$[16] and $Ru_7(CO)_{18}(\mu_4\text{-}PPh)_2$[40] resulting from the photochemical activation of metal bonds. These observations do not seem to support a pathway involving loss of CO prior to H_2 addition although a concerted mechanism by which interaction of H_2 occurs simultaneously with CO labilization cannot be a priori ruled out. The remaining mechanistic possibilities are metal–metal bond dissociation and the associative route. Since saturated clusters are regarded as sterically protected systems, the initial addition of H_2 must take place either with concomitant scission of a metal–metal bond or with a weakening of the metal cluster bonding. On the basis of the high yield of $(\mu\text{-}H)_2Ru_4(CO)_{12}(\mu_3\text{-}PPh)$ and the lack of side products arising from M–M bond cleavage, the last alternative is quite conceivable, especially as a substantial number of 64-electron complexes adopt geometries in which weak and strong M–M interactions combine up to a net total of four normal bonds.[41]

^{13}C NMR Studies

The room-temperature (298 K) $^{13}C\{^1H\}$ spectrum of **2** consisted of three sharp resonances (δ 200.2, 196.1, 185.5 ppm) and two broad signals (δ 199.0, 189.0 ppm), indicative of dynamic behavior. An unambiguous assignment and the nature of the carbonyl interchange processes were revealed by a variable-temperature study. A representative set of $^{13}C\{^1H\}$ spectra from 198 to 298 K is illustrated in Figure 2.

At 233 K, six sharp resonances (δ 200.2, 199.2, 196.1, 189.8, 187.5, 185.6 ppm) are distinguishable, suggesting slow carbonyl exchange on the NMR time scale and a static structure. However, this spectrum is not at first sight compatible with the carbonyl environments in the solid-state structure (Figure 1), which contains a pseudomirror plane through Ru(3), Ru(2), and P(1). Lower temperature spectra displayed a further fluxional process. Below 233 K, the high-field resonance (δ 200.2 ppm) begins to broaden, and at the lowest temperature accessible (198 K), the signal disappears into the baseline (Figure 2). The discovery of this

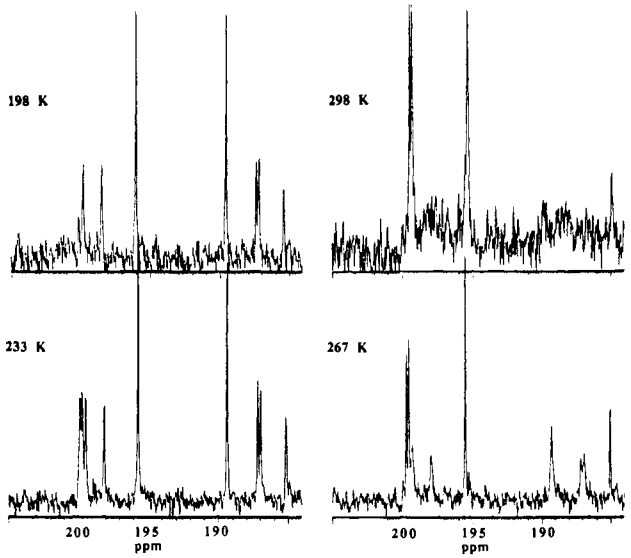

Figure 2. Variable-temperature $^{13}C\{^1H\}$ NMR spectra of $(\mu\text{-}H)_2Ru_4(CO)_{12}(\mu_3\text{-}PPh)$ (**2**) in the carbonyl region.

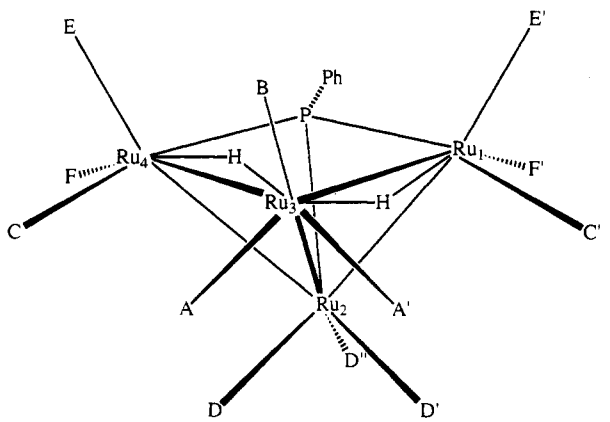

Figure 3. Carbonyl-labeling scheme of $(\mu\text{-}H)_2Ru_4(CO)_{12}(\mu_3\text{-}PPh)$ (**2**).

dynamic process, even though it could not be frozen out, together with an examination of proton-coupled ^{13}C spectra allowed a consistent assignment of each individual ^{13}CO resonance. The labeling scheme for the seven unique carbonyl sites is shown in Figure 3.

The signal at δ 199.2 ppm shows the largest coupling to phosphorus ($^2J_{PC}$ = 67 Hz) and is characteristic of a carbonyl ligand approximately trans to phosphorus. This resonance is assigned to sites C and C′ (Figure 3), which correspond to the C(2) and C(11) carbonyl groups (P(1)–Ru(1)–C(2) = 158.9 (2)°; P(1)–Ru(4)–C(11) = 157.0 (2)°) in Figure 1. The signal at δ 196.1 ppm is strongly coupled to both hydride ligands ($^2J_{CH}$ = 13.5, 4 Hz) and is split into a doublet of doublets in the ^1H-coupled ^{13}C spectrum. This peak is ascribed to the two equivalent carbonyls A and A′ bound to Ru(3) and located trans to the hydride ligands bridging the hinge to wingtip Ru–Ru bonds. A coupling of similar magnitude (J_{CH} = 13 Hz) has been observed for CO ligands in the heterometallic cluster $(\mu\text{-}H)FeRu_3(CO)_{12}(\mu_4\text{-}N)$.[42]

Examination of the evolution of the exchange process with increasing temperature (Figure 2) revealed that the CO ligands associated with resonances at δ 196.1 and 185.6 ppm started to exchange at much higher temperatures than the remaining CO ligands, this behavior being evident only with the broadening of these signals at 298 K. Having already assigned the δ 196.1 ppm resonance to A and A′, we can confidently assign the δ 185.6 ppm

(37) Adams, R. D.; Wang, S. *Inorg. Chem.* **1986**, *25*, 2534.
(38) Adams, R. D.; Horvath, I. T. *Prog. Inorg. Chem.* **1986**, *33*, 127.
(39) After 5 days, 75% of the starting material had been consumed but only 28% of **2** was recovered, the major other products being $(\mu\text{-}H)_2Ru_3(CO)_{12}(\mu_3\text{-}PPh)$ and $Ru_3(CO)_{12}$.
(40) Van Gastel, F.; Taylor, N. J.; Carty, A. J. *J. Chem. Soc., Chem. Commun.* **1987**, 1049.
(41) (a) Carty, A. J.; MacLaughlin, S. A.; Van Wagner, J.; Taylor, N. J. *Organometallics* **1982**, *1*, 1013. (b) Hogarth, G.; Philipps, J. A.; Van Gastel, F.; Taylor, N. J.; Marder, T. B.; Carty, A. J. *J. Chem. Soc., Chem. Commun.* **1988**, 1570. (c) Johnston, V. J.; Einstein, F. W. B.; Pomeroy, R. K. *J. Am. Chem. Soc.* **1987**, *109*, 7220. (d) Martin, L. R.; Einstein, F. W. B.; Pomeroy, R. K. *Organometallics* **1988**, *7*, 294.
(42) Blohm, M. L.; Fjare, D. E.; Gladfelter, W. L. *J. Am. Chem. Soc.* **1986**, *108*, 2301.

peak to B. The high-energy dynamic process represents trigonal rotation at Ru(3), and the higher barrier to rotation at this site is consistent with the presence of bridging hydrides at Ru(3).

Over the temperature range 198–233 K, the sharp doublet at δ 200.15 ppm ($^2J_{PC}$ = 8.5 Hz) began to broaden and at 218 K was a very broad singlet, indicating the presence of a low-energy exchange mode. This time-averaged signal of intensity 3 is a result of rapid trigonal rotation of three CO ligands and can be attributed to carbonyls D, D′, and D″ (Figure 3).

When the temperature was raised from 233 K, the resonances at δ 199.2 (already assigned to C and C′), 189.8, and 187.5 ppm all began to broaden simultaneously. The two higher field signals must therefore belong to the four remaining wingtip CO ligands. The signal at 187.5 ppm exhibited coupling to ^{31}P ($^2J_{PC}$ = 10.5 Hz) and appeared as a doublet in the $^{13}C\{^1H\}$ spectrum. The same resonance displayed a pseudotriplet in the ^{1}H-coupled ^{13}C spectrum, indicating $^2J_{CH}$ and $^2J_{PC}$ couplings of similar magnitude. The absence of proton coupling for the singlet δ 189.8 ppm allows the attribution of the signal at δ 187.5 ppm to sites F and F′, which are approximately trans to the hydride ligands (C(3) and C(12) in Figure 1), as long as the latter do not move over the cluster surface. This is borne out by the fact that the variable-temperature ^{1}H NMR spectra of the heterometallic analogue $(\mu\text{-H})_2Os_3Ru(CO)_{12}(\mu_3\text{-}PC_6H_{11})$ indicate that the inequivalent hydrides of the isomer with the Ru atom located at a wingtip position begin to exchange only at 340 K.[23] The remaining resonance at δ 189.8 ppm is therefore due to carbonyls E and E′. This assignment substantiates empirical observations on the angular dependence of $^2J_{PC}$ coupling constants which seem to suggest a near-zero value for P–M–C bond angles close to 110°.[43]

There are thus three distinct CO exchange processes in **2**. The first and lowest energy process is trigonal rotation at Ru(2). At intermediate temperatures, the wingtip carbonyls begin to convert via a similar mode, and at room temperature, the onset of exchange of carbonyls at the hydride-bound site Ru(3) is observable. In the temperature range accessible without sample decomposition, no intermetallic CO transfer is evident, all of the dynamic processes being localized exchanges.

Acknowledgment. We are grateful to the Natural Sciences and Engineering Research Council for finanical support of this work and to the Government of Ontario for a scholarship (to J.F.C.). The award of an R. G. Goel Scholarship to F.V.G. by the Guelph-Waterloo Centre for Graduate Work in Chemistry is gratefully acknowledged.

Supplementary Material Available: Tables S1–S5, listing anisotropic thermal coefficients, all interatomic distances and bond angles, H atom positional parameters, and complete crystallographic data for **2**, and Figure S1, showing the $^{13}C\{^1H\}$ NMR spectra for **2** over the temperature range 198–298 K (9 pages). Ordering information is given on any current masthead page.

Registry No. **1**, 81726-80-9; **2**, 143345-54-4; cyclohexene, 110-83-8.

(43) Randall, L. H.; Cherkas, A. A.; Carty, A. J. *Organometallics* **1989**, *8*, 568. The trend observed for phosphido-bridged systems is that $^2J_{PC}$ coupling constants appear to minimize at P–M–C bond angles of 90° and maximize at 180° with a sign inversion occurring near angles of approximately 107°. In **2**, the P–M–C angles are on average 91.6° for sites F and F′ and 106.1° for E and E′.